

Recurrence rate and magma effusion rate for the latest volcanism on Arsia Mons, Mars

1 Introduction

Greeley and Schneid [1991] produced one of the first extrusive magma flux estimates for the surface of Mars and used terrestrial intrusive/extrusive ratios to calculate that $6.5 \cdot 10^8 \text{ km}^3$ of magma has been generated on Mars in the past 3.8 Ga. For the most recent 500 Ma, magma production was observed to wane, and only $2.11 \cdot 10^6 \text{ km}^3$ of magma was modeled to have erupted [Greeley and Schneid, 1991]. This global extrusive magma flux of $0.004 \text{ km}^3/\text{yr}$ ($0.13 \text{ m}^3/\text{s}$) remains one of few such estimates of magma production. Constraining past and recent magma production and extrusion rates, however, is of vital importance in understanding evolution of the Martian climate [Mouginis-Mark and Rowland, 2008, Halevy and Head III, 2014, e.g.], lithosphere and mantle [Grott et al., 2013], surface [Wilson and Head, 1994], and the ability of Mars to sustain biotic or pre-biotic material over time [Scanlon et al., 2015b].

The large volcanic edifices of the Tharsis region have been given a time-averaged magma flux estimate of $0.05 \text{ m}^3/\text{s}$, with a factor of 3 uncertainty, for an active construction period of 1 Gyr (again with a factor of 3 uncertainty) by Wilson et al. [2001]. Wilson et al. [2001] further constrained periodic flux under these volcanoes by assuming each of the many summit calderas was formed in association with one stable magma body at depth. By calculating the necessary flux to achieve the magma bodies that could form such calderas, Wilson et al. [2001] found that the magma delivery rate to the volcanoes had to persist at $1\text{-}10 \text{ m}^3/\text{s}$ for hundreds of thousands to millions of years, followed by orders of magnitude longer periods of quiescence before new large magma bodies could be emplaced. For example, assuming a magma chamber size of $50,000 \text{ km}^3$ under the Arsia Mons caldera [Wilson et al., 2001], it would take a $10 \text{ m}^3/\text{s}$ magma flux 140 kyr to fill the magma chamber, representing $\sim 3\%$ of Arsia's total volume in just 0.01% of a 1 Gyr constructional period.

We seek to estimate both the recurrence rate of volcanism and the extrusive magma delivery rate for the most recent volcanic unit on Arsia Mons—a patchwork of lava flows and 29 associated volcanic vents within the volcano caldera. To constrain these values, absolute ages and associated age uncertainty of each flow have been modeled using the size-frequency distribution of observed craters, relative ages between flows have been determined using superposition relationships, and volumes have been modeled using Mars Orbiter Laser Altimeter (MOLA) data [Smith et al., 2003]. Crater-retention age models and stratigraphic relations are integrated in a Volcanic Event Recurrence Rate Model (VERRM) to better

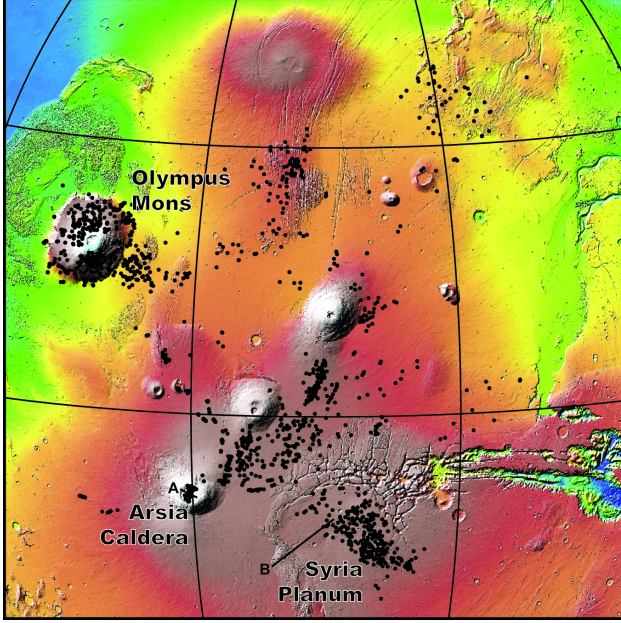


Figure 1: The Tharsis Volcanic Province of Mars. Each black dot represents one small volcanic vent in a Tharsis-wide catalog. Within Arsia Mons (bottom left), 29 vents have been identified. The color relief basemap is MOLA topography.

characterize event age uncertainty and estimate recurrence rate throughout the period of time during which these lavas were emplaced.

2 Geologic Background of Arsia Mons

Arsia Mons is a major shield volcano on Mars and a member of the Tharsis Montes (Figure 1). With a diameter of over 300 km and slopes of 5° [Plescia, 2004], the surface of Arsia contains lava flows, which served as the primary construction material of the shield [Mouginis-Mark and Rowland, 2008], prodigious ash deposits [Mouginis-Mark, 2002], and glacial deposits [Head and Marchant, 2003] emplaced under both cold- and warm-based glacial conditions [Scanlon et al., 2015b]. At the summit of Arsia is a single collapse caldera measuring ~ 4000 km^3 in volume [Wilson et al., 2001]. Within this 110 km wide caldera, a linear cluster of secondary shield volcanoes comprise one of the youngest geologic units in the Arsia region [Carr et al., 1977, Scott and Zimbelman, 1995]. No craters larger than 1 km exist within the caldera and several detailed crater retention studies with different image datasets have independently produced 130 Ma as a single age estimate of the entire caldera floor [Neukum et al., 2004, Werner, 2009, Robbins et al., 2011].

Through Mariner 9 and Viking Orbiter images of the Tharsis region, Crumpler and Aubele [1978] determined that of the three Tharsis Montes, Arsia Mons is the most structurally evolved shield volcano. This conclusion was backed up by Bleacher et al. [2007a] with extensive mapping using HRSC and THEMIS. Bleacher et al. [2007a] suggested that the northward trending structural complexity of the Tharsis Montes might indicate a migrating magma source along the axis of the three volcanoes, similar to a Tharsis plume model

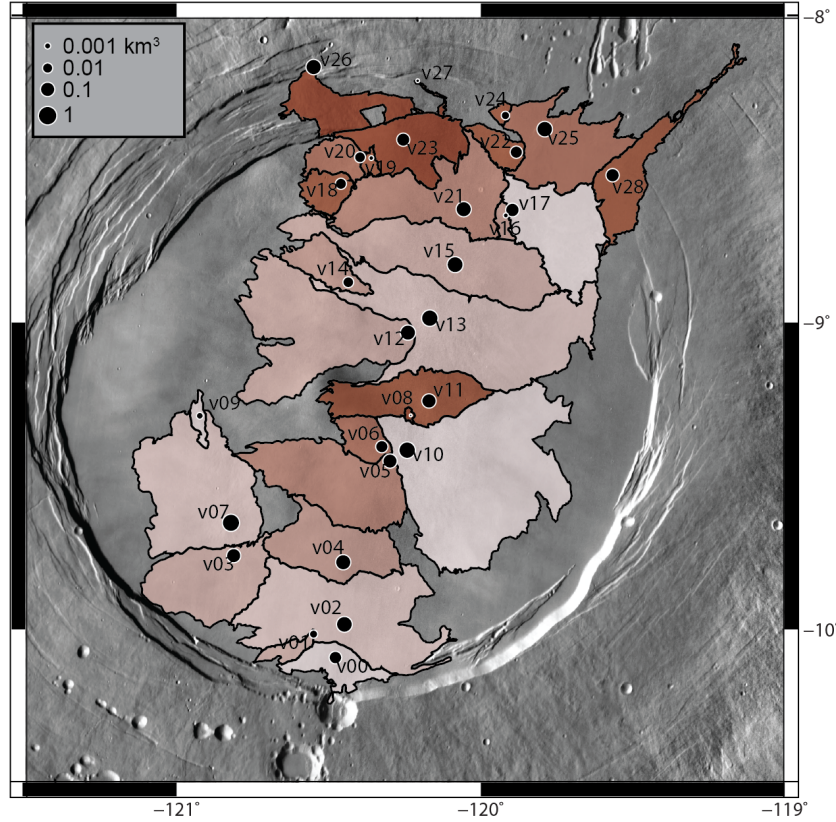


Figure 2: Mapped lava flows in the vent field. Circles are placed at the 29 vent locations and are sized according to volume. Lighter colored flows are higher stratigraphically than darker colored flows (See Figure 3).

by Mège and Masson [1996]. If such a migrating magma source did exist, then magma production at Arsia would have waned, decreasing the amount of melt available for continued summit volcanism.

On the flank of Arsia Mons, Mouginis-Mark and Rowland [2008] identified >1000 layered units in a graben, which were interpreted to be lava flows. Using MOLA data, they were able to estimate the height of the graben wall, enabling the estimation of layer thicknesses between 10-80 m, with most being >30 m. As no unique and laterally extensive layers were observed in the stack of <2 km wide layers, Mouginis-Mark and Rowland [2008] concluded that no major glacial events were emplaced between the deposition of these layers, perhaps indicating relatively rapid emplacement of 885 m of lava. By instead assuming constant activity of Arsia Mons for either 2 or 3 billion years, Mouginis-Mark and Rowland [2008] estimated that the stack could have been emplaced over 290 or 435 million years, respectively.

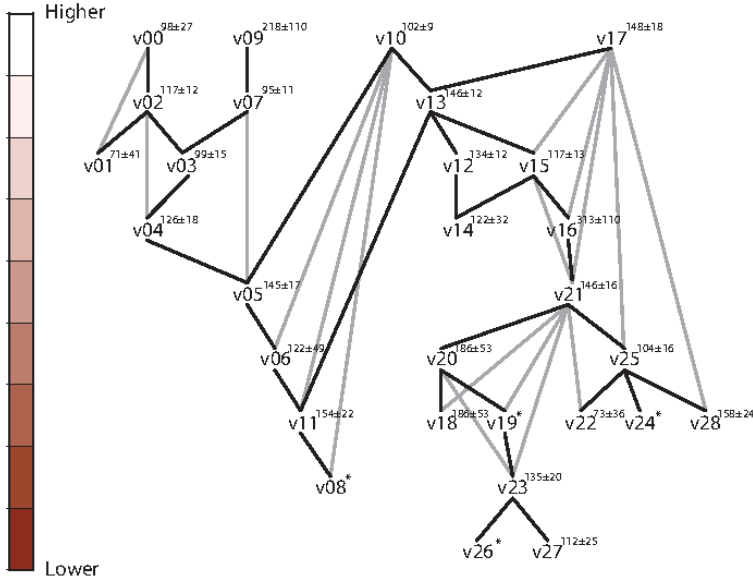


Figure 3: Stratigraphic relationships within the Arsia Mons Caldera. Higher flows (e.g. v00) are higher stratigraphically. Each line is one stratigraphic relationship connecting an overlying and an underlying flow. Gray lines are mapped, but can be inferred indirectly by other relationships. Age estimates from craterstats2 are given in superscript; * symbols indicate no age was estimated due to a lack of craters with $D \geq 100$ m.

3 Methods

3.1 Unit and stratigraphic mapping

The 29 mapped volcanic vents within the caldera each have lava flows emanating from them that form positive topographic features over the surrounding terrain. Flows corresponding to each vent have been mapped in ArcGIS 10.2 with georeferenced Context Imager (CTX) photographs [Malin et al., 2007] serving as a 6-m resolution basemap (Figure 2). Flows are mapped in association with an observed vent where flows can be unambiguously traced directly back to the vent using flow features. Some lava flows on the eastern and western margins of the caldera appear to flow away from the caldera center and might have been created during an event that formed any of the observed vents; however, because they are covered in subsequent flows and are separated from their parent vent by at least one flow front, they cannot be traced to a vent and are not included in our catalog.

Mapped flows which abut each other have an inherent superposition relationship. Using available CTX images, these relationships are documented for all neighboring flows by identifying features such as 1) diverted flows around pre-existing topography, 2) infilling of graben or volcanic vents, and 3) continuous flow features suddenly vanishing under overlying flows. Superposition relationships are graphed according to stratigraphic height in Figure 3.

3.2 Crater retention age modeling

Mapped units within the caldera (29 lava flow units and 1 “undifferentiated lavas” unit) have been assigned model ages based on the distribution of impact craters within their boundaries. Robbins et al. [2011] previously found that, in the Arsia Mons caldera, crater frequency decreases for craters with diameters (D) of ≤ 93 m, due to dust cover. Robbins et al. [2011] also hypothesized that a background population of secondary craters in this area might contaminate the crater distribution at $D < 130$ m. We have counted all craters in the caldera with $D \geq 100$ m to avoid both of these systematic biases. Four lava flows have an exposed area smaller than 15 km^2 and an insignificant number of craters larger than 100 m were found on their surfaces (10 or fewer), so no crater age date was determined. The diameter and location of craters were mapped in ArcGIS 10.2 using a basemap of CTX images.

Modeled ages based on a impact production function, which is a model of the relative production rate of different impact crater sizes, and a chronology function, which models the change of impact frequency with time. Ages were modeled in the Craterstats2 software [Michael, 2013]. For each mapped unit, craters are separated by diameter into bins of minimum diameter $2d$ km where d increments by 0.5 between each bin, following the Hartmann 2004 iteration Production Function [Hartmann, 2005]. Ages are modeled based on this Production Function and the Michael [2013] Chronology Function. Uncertainty of crater frequency in each bin is defined as \sqrt{N}/S , where N is the number of craters and S is the area of the mapped unit. The cumulative crater-size frequency distribution (and associated uncertainty) is assembled from each $2d$ km bin and is used to model a best fit age (see Figure 7). Ages and uncertainties for each mapped unit are reported in Ma.

For the four small flows where craters at $D > 30$ m have been counted, the crater frequency roll-off is observed to occur between 35 and 60 m. To model the ages of these flows, only craters larger than this roll-off diameter are included. If a background population of secondary craters ≥ 130 m is present, the cumulative crater-size frequency distribution should have an increased slope below this diameter. This slope increase was not visually seen in individual mapped units, though if it is present then the four small flows will have modeled ages that are older than the actual flow age.

3.3 Volume estimation

Two volume estimation methods are used to provide minimum and maximum volume constraints for each lava flow (Figure 5). A primary initial assumption of these methods is that the erupted material was predominantly effusive, while insignificant material would have been advected far from the source.

First, volumes are estimated for each individual flow. Elevation values are assigned to the mapped perimeter of each flow from the gridded-MOLA topographic dataset. The subsurface of the flow is modeled with a triangular irregular network (TIN) where mesh faces are generated with the Delaunay triangulation of vertices along the perimeter. The modeled subsurface is then subtracted from the MOLA grid, producing a thickness map which is integrated to estimate flow volume. This estimate should be considered to be a minimum estimate of flow volume, because the modeled sub-flow surface tightly connects the lava flow

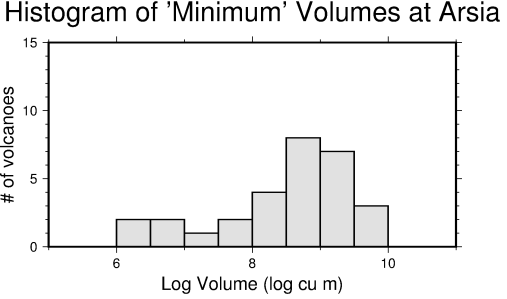


Figure 4: Minimum estimated volumes of each lava flow using an interpolated mesh as a theoretical subsurface. All lavas are estimated to be between 10^{-3} - 1 km^3 , with most volumes centering around 1 km^3 .

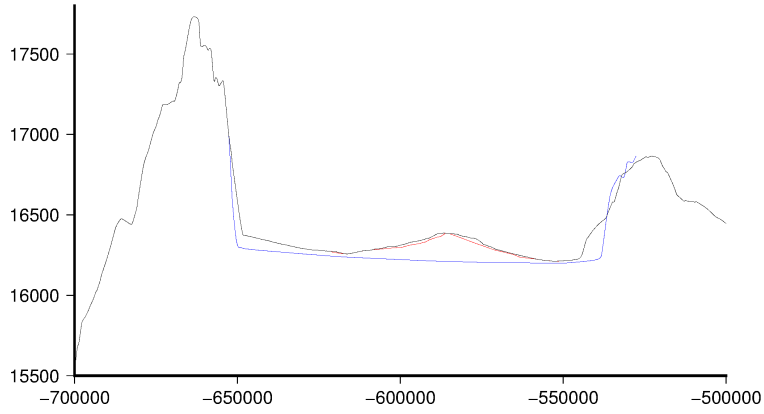


Figure 5: A cross-section of Arsia Mons showing the MOLA topography (black), “minimum estimate” subsurface for two volcanoes (red), and the “maximum estimate” subsurface underlying the entire caldera (blue).

margins, while in real life lava flows invert topography and should likely have a deeper, more concave upward subsurface. Though these volumes are underestimates, their advantage is that they are carried out for each flow.

Second, volume is estimated for the entire caldera using a convex hull of the MOLA topography. The topographic convex hull includes the lowest points in and along the perimeter of the caldera. Points in the hull are again used to model a subsurface using a Delaunay-generated TIN and the volume of the caldera lavas are estimated by subtracting this subsurface from the MOLA topography. Unlike the previous method, this volume cannot easily be divided amongst the mapped flows, might include buried events, and does include distal flows that are not included in the catalog but might correspond to mapped vents. Because of these potential biases, the resulting volume is likely a maximum estimate and does not provide volume estimates for individual events. The estimated caldera volume is therefore divided equally between the 29 mapped vents to provide a maximum estimate.

3.4 Volcanic Event Recurrence Rate Model (VERRM)

Together, stratigraphic information and crater retention age estimates can be consolidated to improve age uncertainty estimation for volcanic events. This is especially applicable to

recent volcanic landforms on Mars as crater-based dates alone might be biased due to crater burial, local topography, or secondary crater background populations [Robbins et al., 2011, Platz and Michael, 2011].

To accomplish the task of constraining modeled age estimates with stratigraphy, and ultimately to describe the repose interval of volcanic events in the region, we have devised an algorithm, which we call the Volcanic Event Recurrence Rate Model (VERRM). VERRM implements a Monte Carlo algorithm that assigns a potential age to each volcanic event by defining an event age distribution function, A , with an event's modeled crater retention rate age and age uncertainty, as reported by Craterstats2. The age distribution function for each event is modeled as a Gaussian distribution, which is a suitable for the events in this study as they are relatively recent and the crater impact rate during the time of their emplacement is thought to be constant [Vaucher et al., 2009]. The initial age function is given as $A_i(\mu_i, \sigma_i^2)$ where μ is the estimated age determined by crater retention and σ is the uncertainty of the estimated age of cataloged event i . VERRM then constrains A with a binary stratigraphy function, with possible ages having a value of 1 and ages outside an acceptable age range having a value of 0. Possible ages are defined by previously dated events in the VERRM simulation; stratigraphically higher events connected to the event at hand give a minimum age of the stratigraphy function, while lower events give a maximum age. If no stratigraphically-related events have been dated, the minimum age bound is set to the present, and the maximum age bound is set to three times older than the oldest crater retention rate modeled age in this field (330 Ma), or 1 Ga.

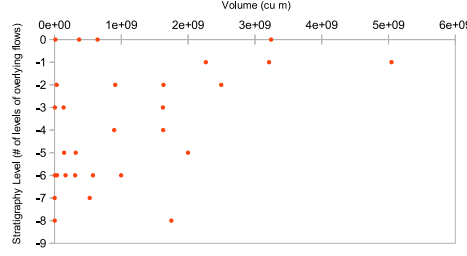
The normalized product of the Gaussian age function and the binary stratigraphy function gives an age distribution function which does not violate stratigraphy but is informed by crater retention age estimates. This function is sampled to date an event and the process repeats for the next event. By repeating this process 10,000 times, the potential age ranges for each event is determined.

Recurrence Rate

Volumes

4 Results

The 29 lava flows in our catalog are mapped to cover 6700 km^2 , $\sim 70\%$, of the caldera, representing the majority of surface lavas within the caldera walls (Figure 2). Individual lava flow volume estimates range from $1.6 \cdot 10^{-3}$ to 5 km^3 , with an average of 1.1 km^3 per flow (Figure 4). Buried flows are, on average, smaller in volume, but not all stratigraphically lower flows are small in volume (Figure 6). The total volume using the individual volume estimations, again assumed to be a minimum, is 31 km^3 . The total volume using the convex hull approach over the entire caldera is 400 km^3 . This estimate is more than an order of magnitude larger than the minimum volume estimate and would mean each vent expelled roughly 13 km^3 of lava. Results for each lava flow are recorded in Table (1).



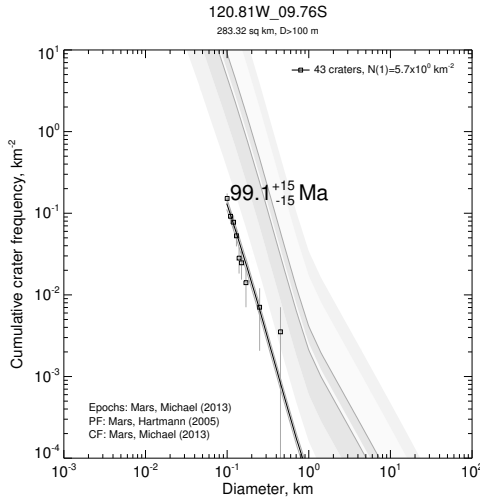


Figure 7: An example cumulative crater frequency distribution. This flow (v03) had been previously estimated to be 97 ± 49 Ma from crater counting performed on a HiRISE image [Robbins et al., 2011]. Our age of 99 ± 15 Ma agrees with this previous finding.

flux necessary to sustain a magma chamber, but is only one order of magnitude smaller than the average flux needed to build Arsia Mons in 1 Gyr, $0.05 \text{ m}^3 \text{ s}^{-1}$ [Wilson et al., 2001].

Time-averaged recurrence can be estimated by dividing the total elapsed time of volcanic activity by number of events. For instance, Richardson et al. [2013] identified 263 monogenetic volcanic vents within Syria Planum, which were interpreted to be emplaced from 3.6-2.9 Ga, or 700 Myr. If volcanism were constant in that area, a new volcanic vent would have been formed every 2.7 Myr. In a graben on the northwest flank of Arsia, Mouginis-Mark and Rowland [2008] mapped >1000 lava flows and estimated construction rates of 290 and 435 million years, based on the time to build all of Arsia Mons. This would correspond to a recurrence of at least one episode of lava emplacement every 290 or 440 kyr. A time-averaged recurrence for our 29 vents, created over 230 Myr, would be one event every 8 Myr. This alone would imply that the latest volcanic activity on Arsia Mons was much closer in style to the volcanism on Syria Planum than during the main constructional phases of Arsia Mons.

5.2 Effects on tropical mountain glaciers on Arsia Mons

In the past decade, studies have interpreted fan-shaped deposits on the western flanks of the Tharsis Montes to be recent glacial deposits, due to the presence of fresh moraines and possible stranded ice blocks, analogous to kettles on Earth [Shean et al., 2007, Kadish et al., 2014, Scanlon et al., 2015a]. The material on these broad deposits have been dated by Kadish et al. [2014] to have been emplaced around 200 Ma. Scanlon et al. [2015b] identified fan-shaped deposits on the western flank of Arsia Mons which contain evidence of basal melting in clear association with sub-glacial volcanic eruptions.

Recent analysis of smooth facies deposits to the northwest of the Arsia summit has provided evidence that tropical mountain glaciers are, in fact, extant and covered in ash [Scanlon et al., 2015a]. The penetration depth of viscously relaxed ring-mold craters on these deposits indicates a maximum material blanket thickness of less than 230 m over tens to hundreds of meters of ice or ice-rich material [Head and Weiss, 2014]. A large portion of this insulating material might in fact be volcanic ash [Wilson and Head, 1994; Mouginis-Mark, 2002].

The presence of volcanic ash on remaining tropical mountain glaciers on the flank of Arsia might be a result of the most recent volcanism in the Arsia caldera. If this is the case, our volume estimates would likely be severely underestimated, as a large portion of erupted material would have been transported away from the vent as tephra. However, as Kadish et al. [2014] estimated the resurfacing age of the fan-shaped deposits to be about 200 Ma, roughly our interpreted age of onset of effusive activity within the caldera, it is possible that the ash on the flanks and the lavas in the caldera represent a transition from explosive to effusive volcanism at Arsia Mons. The provenance of the ash might be buried by the recent lavas or might be the “parasitic calderas” observed by Crumpler et al. [1996], which form a rift of the south and north caldera walls of Arsia, in line with the shield volcanoes in our catalog.

5.3 Other recent volcanism in the Tharsis Region

If recent Arsia volcanism transitioned from explosive to effusive at about 200 Ma, it might be analogous to transitions in eruption dynamics at other major volcanic edifices on Mars. The latest lava flows on the flanks of Olympus Mons appear to have also changed from long tube-fed flows to shorter, channel-fed flows, suggesting that magma flux per flow emplacement event has waned over the late Amazonian [Bleacher et al., 2007b]. Bleacher et al. [2007b] concluded that this might be evidence of a larger waning of activity at Olympus and might also signal a transition from a deep mantle source of volcanism to shallower sources, based on long-term volcanic patterns observed at the Hawaiian volcanic chain. While the morphologies of the most recent lava flows on Arsia and Olympus might both indicate waning magma production, these observations might be consistent with the Wilson et al. [2001] model that most of the history of these volcanoes is spent dormant after hyper-active edifice building episodes wane and end.

Volcanism elsewhere in Tharsis has occurred recently in a more distributed fashion [Hauber et al., 2011], including a lava field filling the southeast “moat” of Olympus Mons [Chadwick et al., 2015]. Indeed, Chadwick et al. [2015] identified lava flows at the base of Olympus emplaced between 64–210 Ma, roughly during the same period as the lava flows in this study. The emplacement direction of these lavas are systematically offset from the current downward direction, due to recent subsidence of Olympus Mons. The required magma to be injected in the past 200 Myr into Olympus Mons to cause this subsidence might be 10^5 – 10^6 km 3 [Chadwick et al., 2015], suggesting that the large volcanoes of the Tharsis Region are not yet extinct.

References

- SM Baloga, PJ Mouginis-Mark, and LS Glaze. Rheology of a long lava flow at pavonis mons, mars. *Journal of Geophysical Research: Planets*, 108(E7), 2003. doi: 10.1029/2002JE001981.
- Jacob E. Bleacher, R. Greeley, D. A. Williams, S. R. Cave, and G. Neukum. Trends in effusive style at the Tharsis Montes, Mars, and implication for the development of the Tharsis province. *Journal of Geophysical Research*, 112:E09005, 2007a. doi: 10.1029/2006JE002873. doi:10.1029/2006JE002873.
- Jacob E Bleacher, Ronald Greeley, David A Williams, Stephanie C Werner, Ernst Hauber, and Gerhard Neukum. Olympus mons, mars: Inferred changes in late amazonian aged effusive activity from lava flow mapping of mars express high resolution stereo camera data. *Journal of Geophysical Research: Planets*, 112(E4), 2007b. doi: 10.1029/2006JE002826.
- M. H. Carr, R. Greeley, K. R. Blasius, J. E. Guest, and J. B. Murray. Some Martian volcanic features as viewed from the Viking orbiters. *Journal of Geophysical Research*, 82: 3985–4015, 1977.
- John Chadwick, Patrick McGovern, Mariel Simpson, and Ashleigh Reeves. Late amazonian subsidence and magmatism of olympus mons, mars. *Journal of Geophysical Research: Planets*, 2015. doi: 10.1002/2015JE004875.
- LS Crumpler and JC Aubele. Structural evolution of Arsia Mons, Pavonis Mons, and Ascreus Mons: Tharsis region of Mars. *Icarus*, 34(3):496–511, 1978. doi: 10.1016/0019-1035(78)90041-6.
- LS Crumpler, James W Head, and Jayne C Aubele. Calderas on mars: Characteristics, structure, and associated flank deformation. *Geological Society, London, Special Publications*, 110(1):307–348, 1996. doi: 10.1144/GSL.SP.1996.110.01.24.
- Lori S Glaze, Stephen M Baloga, and Ellen R Stofan. A methodology for constraining lava flow rheologies with mola. *Icarus*, 165(1):26–33, 2003. doi: 10.1016/S0019-1035(03)00171-4.
- Ronald Greeley and Byron D Schneid. Magma generation on mars: Amounts, rates, and comparisons with earth, moon, and venus. *Science*, 254(5034):996, 1991. doi: 10.1126/science.254.5034.996.
- Matthias Grott, David Baratoux, Ernst Hauber, V Sautter, J Mustard, O Gasnault, Steven W Ruff, S-I Karato, Vinciane Debaille, Martin Knapmeyer, et al. Long-term evolution of the martian crust-mantle system. *Space science reviews*, 174(1-4):49–111, 2013. doi: 10.1007/s11214-012-9948-3.
- Itay Halevy and James W Head III. Episodic warming of early mars by punctuated volcanism. *Nature Geoscience*, 2014. doi: 10.1038/ngeo2293.

William K. Hartmann. Martian cratering 8: Isochron refinement and the chronology of Mars. *Icarus*, 174(2):294 – 320, 2005. ISSN 0019-1035. doi: 10.1016/j.icarus.2004.11.023. doi:10.1016/j.icarus.2004.11.023.

E. Hauber, P. Brož, F. Jagert, P. Jodłowski, and T. Platz. Very recent and wide-spread basaltic volcanism on Mars. *Geophysical Research Letters*, 38:L10201, 2011. doi: 10.1029/2011GL047310. doi:10.1029/2011GL047310.

James W Head and David R Marchant. Cold-based mountain glaciers on mars: western arsia mons. *Geology*, 31(7):641–644, 2003. doi: 10.1130/0091-7613(2003)031<0641:CMGOMW>2.0.CO;2.

James W Head and David K Weiss. Preservation of ancient ice at pavonis and arsia mons: tropical mountain glacier deposits on mars. *Planetary and Space Science*, 103:331–338, 2014. doi: 10.1016/j.pss.2014.09.004.

H Hiesinger, JW Head, and G Neukum. Young lava flows on the eastern flank of ascraeus mons: Rheological properties derived from high resolution stereo camera (hrsc) images and mars orbiter laser altimeter (mola) data. *Journal of Geophysical Research: Planets*, 112(E5), 2007. doi: 10.1029/2006JE002717.

Seth J Kadish, James W Head, James L Fastook, and David R Marchant. Middle to late amazonian tropical mountain glaciers on mars: The ages of the tharsis montes fan-shaped deposits. *Planetary and Space Science*, 91:52–59, 2014. doi: 10.1016/j.pss.2013.12.005.

Michael C. Malin, James F. Bell, Bruce A. Cantor, Michael A. Caplinger, Wendy M. Calvin, R. Todd Clancy, Kenneth S. Edgett, Lawrence Edwards, Robert M. Haberle, Philip B. James, Steven W. Lee, Michael A. Ravine, Peter C. Thomas, and Michael J. Wolff. Context Camera Investigation on board the Mars Reconnaissance Orbiter. *Journal of Geophysical Research*, 112(E5):E05S04, 2007. doi: 10.1029/2006JE002808. doi:10.1029/2006JE002808.

D. Mège and P. Masson. A plume tectonics model for the Tharsis Province, Mars. *Planetary and Space Science*, 44:1499–1546, 1996.

GG Michael. Planetary surface dating from crater size-frequency distribution measurements: Multiple resurfacing episodes and differential isochron fitting. *Icarus*, 226(1):885–890, 2013. doi: 10.1016/j.icarus.2013.07.004.

Peter J Mouginis-Mark. Prodigious ash deposits near the summit of arsia mons volcano, mars. *Geophysical research letters*, 29(16):15–1, 2002. doi: 10.1029/2002GL015296.

Peter J Mouginis-Mark and Scott K Rowland. Lava flows at arsia mons, mars: Insights from a graben imaged by hirise. *Icarus*, 198(1):27–36, 2008. doi: 10.1016/j.icarus.2008.06.015.

G. Neukum, R. Jaumann, H. Hoffmann, E. Hauber, J. W. Head, A. T. Basilevsky, B. A. Ivanov, S. C. Werner, S. van Gasselt, J. B. Murray, T. McCord, and The HRSC Co-Investigator Team. Recent and episodic volcanic and glacial activity on Mars revealed by the High Resolution Stereo Camera. *Nature*, 432(7020):971–979, 2004. doi: 10.1038/nature03231. doi:10.1038/nature03231.

Jan Hendrik Pasckert, Harald Hiesinger, and Dennis Reiss. Rheologies and ages of lava flows on elysium mons, mars. *Icarus*, 219(1):443–457, 2012. doi: 10.1016/j.icarus.2012.03.014.

Thomas Platz and Gregory Michael. Eruption history of the elysium volcanic province, mars. *Earth and Planetary Science Letters*, 312(1):140–151, 2011. doi: 10.1016/j.epsl.2011.10.001.

J. B. Plescia. Morphometric properties of Martian volcanoes. *Journal of Geophysical Research*, 109(E3):E03003, 2004. doi: 10.1029/2002JE002031. doi:10.1029/2002JE002031.

Jacob A Richardson, Jacob E Bleacher, and Lori S Glaze. The volcanic history of syria planum, mars. *Journal of Volcanology and Geothermal Research*, 252:1–13, 2013. doi: 10.1016/j.jvolgeores.2012.11.007.

Stuart J Robbins, Gaetano Di Achille, and Brian M Hynek. The volcanic history of mars: High-resolution crater-based studies of the calderas of 20 volcanoes. *Icarus*, 211(2):1179–1203, 2011. doi: 10.1016/j.icarus.2010.11.012.

Kathleen E Scanlon, James W Head, and David R Marchant. Remnant buried ice in the equatorial regions of mars: Morphological indicators associated with the arsia mons tropical mountain glacier deposits. *Planetary and Space Science*, 111:144–154, 2015a. doi: 10.1016/j.pss.2015.03.024.

Kathleen E Scanlon, James W Head, and David R Marchant. Volcanism-induced, local wet-based glacial conditions recorded in the late amazonian arsia mons tropical mountain glacier deposits. *Icarus*, 250:18–31, 2015b. doi: 10.1016/j.icarus.2014.11.016.

David Holcomb Scott and James R Zimbelman. Geologic map of arsia mons volcano, mars. Technical Report IMAP 2480, USGS, 1995.

David E Shean, James W Head, James L Fastook, and David R Marchant. Recent glaciation at high elevations on arsia mons, mars: Implications for the formation and evolution of large tropical mountain glaciers. *Journal of Geophysical Research: Planets*, 112(E3), 2007. doi: 10.1029/2006JE002761.

D. E. Smith, M. T. Zuber, G. A. Neumann, E. A. Guinness, and S. Slavney. Mars Global Surveyor Laser Altimeter Mission Experiment Gridded Data Record. NASA Planetary Data System, MGS-M-MOLA-5-MEGDR-L3-V1.0., 2003.

J Vaucher, D Baratoux, N Mangold, P Pinet, K Kurita, and M Grégoire. The volcanic history of central elysium planitia: Implications for martian magmatism. *Icarus*, 204(2): 418–442, 2009. doi: 10.1016/j.icarus.2009.06.032.

Stephanie C Werner. The global martian volcanic evolutionary history. *Icarus*, 201(1):44–68, 2009. doi: 10.1016/j.icarus.2008.12.019.

Lionel Wilson and James W Head. Mars: Review and analysis of volcanic eruption theory and relationships to observed landforms. *Reviews of Geophysics*, 32(3):221–263, 1994. doi: 10.1029/94RG01113.

Lionel Wilson, Evelyn D Scott, and James W Head. Evidence for episodicity in the magma supply to the large tharsis volcanoes. *Journal of Geophysical Research: Planets*, 106(E1): 1423–1433, 2001. doi: 10.1029/2000JE001280.

Table 1: Lava Flow Data

Flow	Vent Location Long.	Vent Location Lat.	Area (km ²)	Volume (km ³)	Modeled Age (Ma)	Overlying Flows	Underlying Flows
v00	-120.48°	-10.09°	102.27	0.37	98.4±27	—	02,01
v01	-120.55	-10.02	31.21	0.032	71.4±41	00,02	—
v02	-120.45	-9.98	538.86	2.3	117±12	00	01,03,04
v03	-120.81	-9.76	283.32	0.91	99.1±15	02,07	04
v04	-120.45	-9.78	242.29	1.6	126±18	02,03	05
v05	-120.30	-9.45	353.98	0.89	145±17	04,07,10	06
v06	-120.33	-9.41	69.40	0.31	122±49	05,10	11
v07	-120.82	-9.65	479.32	5.0	94.7±11	09	03,05
v08	-120.23	-9.30	4.00	0.0017	—	11,10	—
v09	-120.92	-9.30	21.08	0.013	218±110	—	07
v10	-120.24	-9.42	858.69	3.2	102±9.3	—	05,06,08,11,13
v11	-120.17	-9.26	228.09	1.0	154±22	06,10,13	08
v12	-120.24	-9.03	528.14	1.6	134±12	13	14
v13	-120.17	-8.99	679.49	3.2	146±12	10,17	12,15,11
v14	-120.44	-8.87	96.78	0.14	122±32	12,15	—
v15	-120.08	-8.81	460.75	2.5	117±13	13,17	14,16,21
v16	-119.92	-8.65	18.11	0.0053	313±110	15,17	21
v17	-119.90	-8.63	300.03	0.64	148±18	—	13,15,16,21,25,28
v18	-120.46	-8.55	64.29	0.16	186±53	20,21	—
v19	-120.36	-8.46	13.12	0.0047	—	20,21	23
v20	-120.40	-8.46	70.51	0.14	186±53	21	18,19,23
v21	-120.06	-8.63	354.97	1.6	146±16	15,16,17	20,18,19,23,22,25
v22	-119.88	-8.44	53.20	0.31	73.2±36	21,25	—
v23	-120.25	-8.40	204.71	0.53	135±20	19,20,21	26,27
v24	-119.92	-8.32	11.70	0.037	—	25	—
v25	-119.79	-8.37	281.19	2.0	104±16	17,21	22,24,28
v26	-120.21	-8.21	5.61	0.0026	—	23	—
v27	-120.55	-8.17	158.16	1.75	112±25	23	—
v28	-119.57	-8.52	176.53	0.58	158±24	17,25	—